World Academy of Science, Engineering and Technology
International Journal of Mechanical and Mechatronics Engineering
Vol:18, No:9, 2024

Drone On-time Obstacle Avoidance for Static and Dynamic Obstacles

Herath MPC Jayaweera, Samer Hanoun

Abstract—Path planning for on-time obstacle avoidance is an essential and challenging task that enables drones to achieve safe operation in any application domain. The level of challenge increases significantly on the obstacle avoidance technique when the drone is following a ground mobile entity (GME). This is mainly due to the change in direction and magnitude of the GME′s velocity in dynamic and unstructured environments. Force field techniques are the most widely used obstacle avoidance methods due to their simplicity, ease of use and potential to be adopted for three-dimensional dynamic environments. However, the existing force field obstacle avoidance techniques suffer many drawbacks including their tendency to generate longer routes when the obstacles are sideways of the drone′s route, poor ability to find the shortest flyable path, propensity to fall into local minima, producing a non-smooth path, and high failure rate in the presence of symmetrical obstacles. To overcome these shortcomings, this paper proposes an on-time three-dimensional obstacle avoidance method for drones to effectively and efficiently avoid dynamic and static obstacles in unknown environments while pursuing a GME. This on-time obstacle avoidance technique generates velocity waypoints for its obstacle-free and efficient path based on the shape of the encountered obstacles. This method can be utilize on most types of drones that have basic distance measurement sensors and autopilot supported flight controllers. The proposed obstacle avoidance technique is validated and evaluated against existing force field methods for different simulation scenarios in Gazebo and ROS supported PX4-SITL. The simulation results show that the proposed obstacle avoidance technique outperforms the existing force field techniques and is better suited for real-world applications.

Keywords—Drones, force field methods, obstacle avoidance, path planning.

I. Introduction

DRONES, also known as unmanned aerial vehicles (UAVs), are machines capable of flying without an onboard pilot. They are broadly utilized by military for intelligent surveillance [1], combat purposes [2], and reconnaissance [3] due to their great advantages, alleviating risks on human pilots and ability to approach places that are too dangerous for humans. In addition to these critical military applications, drones are adopted in the civil domain for forest fire detection [4], crop yield estimation [5], wildlife monitoring [6], disaster response and relief missions [7]. Following GMEs for providing aerial coverage and adequate situational awareness [8] is another important facet of using drones; however, their ability to perform in the above-mentioned applications is highly dependent on their autonomy capabilities and obstacle avoidance abilities when flying at low altitudes that tend to be occupied with different types and shapes of obstacles. Encountered obstacles can be static objects such as tall trees, bridges, high-rise buildings, electric poles, and power lines, and dynamic objects such as birds and other flying drones which can hinder their mission effectiveness while also can cause severe damage to the drone in the case of collisions. Drones efficient path planning can enhance their level of autonomy and successfully help them to avoid obstacles while escaping any kind of potential dangers.

Recently, several on-time drone path planning techniques have been proposed for obstacle avoidance. Artificial Neural Network (ANN) [9], Rapidly Exploring Random Tree (RRT) [10], Genetic Algorithm (GA) [11], Fuzzy Logic (FL) [12], and Artificial Potential Field (APF) [13] are among the prominent approaches. These path planning techniques suffer a common drawback of inability to generate a collision free path if there is uncertainty in the onboard sensory information that is used to access the situational awareness of the drone navigational environment. The effectiveness of the ANN-based path planning [14] relies on the quality and quantity of the data used for training these algorithms; therefore, ANN-based obstacle avoidance [9] has a higher probability of failure in unknown and unstructured dynamic environments due to the lack of prior training in similar scenarios. The RRT [10] methods lack a re-planning procedure and required higher computational power as the computational complexity increases exponentially in obstacle cluttered areas [15]. Although, GA-based techniques are suitable for static obstacle avoidance, they tend to handle dynamic objects poorly due to the insufficient global data [16]. FL techniques [12] generate less smooth and non-optimal paths. The APF-based obstacle avoidance techniques [13] are widely adopted for drone navigation due to their simplicity and effectiveness. The general APF based path planning techniques have several drawbacks including falling in global minima and inability to generate a path in the presence of symmetrical obstacles [17]. However, most of these obstacle avoidance techniques are solely developed for point-to-point drone navigation and cannot be adopted for obstacle avoidance by drones following GMEs without adequate modifications.

Few obstacle avoidance methods have been published in the literature for on-time obstacle avoidance for drones that follow GMEs. Most of them are developed based on the APF techniques by improving their potential functions. The general APF presented in [18] has been modified in [19] by implementing velocity contribution to the potential function for better obstacle avoidance by the drone while following the movements of a GME. However, this method suffers

Herath MPC Jayaweera and Samer Hanoun are with Institute for Intelligent Systems Research and Innovation, Deakin University, Waurn Ponds, VIC 3216, Australia (e-mail: (p.herathmudiyanselage, samer.hanoun)@deakin.edu.au).

many drawbacks including the tendency to produce a longer route when the static obstacles are sideways of the drone route, poor ability to find the shortest path, propensity to fall into local minima, producing a non-smooth path, and high failure rate when symmetrical obstacles are in the drone path. The improved APF called 'dynamic artificial potential field (D-APF)' presented in [20] adapts the drone altitude to prevent collisions while following the GME, but the generated path is usually and unnecessarily longer. Another obstacle avoidance technique has been presented in [8], adopting an improved APF technique to change the horizontal position of the drone while following the movement of the GME. Although, this technique can successfully avoid collisions, the drone is unable to find the most efficient path to maneuver around the obstacles.

To overcome the drawbacks of the existing collision avoidance techniques, this paper proposed an on-time three-dimensional obstacle avoidance method for drones to effectively and efficiently avoid dynamic and static obstacles in unknown complex environment while producing a smooth path for following a GME. This is achieved by modifying the D-APF presented in [20] and introducing a force function for escaping from collision when the obstacles are encountered. The direction of this force is automatically selected based on the shape of the obstacles for generating the minimum distance path. Besides, the activation region of this force from the obstacle is calculated based on the relative velocity between the drone and the nearest obstacle; therefore, unlike the existing force field obstacle avoidance, the proposed technique can adopt for obstacles when the drone is flying with high speed. The proposed escaping force acts perpendicular to the GME heading and the attractive force on the drone acts parallel to the GME heading to control and minimize the oscillations in the presence of obstacles and continue following the GME.

The remaining of the paper is organized as follows. The proposed APF-based obstacle avoidance algorithm including its analytical validation is presented in Section II. The simulation experiments setup is presented in Section III, followed by Section IV on the simulation results for validating the proposed obstacle avoidance technique alongside performance comparison results of the presented obstacle avoidance method to the D-APF and general APFs. Finally, conclusions are present in Section V.

II. Proposed Methodology

The main objective of the drone when following the GME is to provide continuous aerial coverage of the GME by using its onboard sensors. Obstacles that are in the drone's path can hinder its ability to continue following the GME; therefore, a fast and simple obstacle avoidance technique is required to guide the drone to maneuver around the obstacles when obstacles are encountered. APF-based obstacle avoidance techniques are the most commonly used type due to their ease of use, simplicity and effectiveness. The principle behind the APF technique is to create a virtual attractive force to pull the drone towards the goal and, a virtual repulsive force to guide the drone push away from obstacles. The resultant force provides the drone an obstacle-free path to follow the GME in obstacle-occupied environments.

The concept of the proposed collision avoidance method is inspired by the Dynamic Artificial Potential Field (D-APF) method [20]. However, to overcome some of its drawbacks an on-time repulsive force called 'escape force (F_s)', is introduced in a perpendicular direction to the GME heading; therefore, it does not affect the drone's ability to continuously follow the GME. Fig. 1 shows a top view of the proposed collision avoidance path planning force distribution when the drone is following a GME and encountering head-on obstacles where the displacement from the drone to far edge of the obstacle is in the horizontal plane. The heading of F_s is the vector product of $F_a \times -i_z$ for $\alpha_1 < \alpha_2$, and $F_a \times i_z$ for $\alpha_1 \geq \alpha_2$, where α_1 is the angle between the far edge of the obstacle that is on the left side of the drone path. Similarly α_2 is the angle between the far edge of the obstacle that is on the right side of the drone path with respect to the line between the drone and GME. The unit vector in Z direction is denoted as i_z. The i_z is replace from the unit vector i_s which is perpendicular to the direction of F_s and choose the corresponding angles in vertical plane when the displacement between the drone and far edge of the obstacle is in the vertical plane. F_r is the repulsive force that activates only in emergency situations to avoid collision when F_s is unable to escape the obstacle. The resultant force (F_T) acting on the drone is the vector summation of F_a, F_r, and F_s.

The force distribution of the proposed obstacle avoidance technique when the drone is following the GME and encountering a sideway obstacle is shown in Fig. 2. The direction of F_s is calculated based on the angle between F_a and displacement (d_1) between the drone and the obstacle's surface where β_1 is the angle to the left side or right side of F_a. If β_1 is the angle to the left side of F_a, the direction of F_s is given by the vector product of $F_a \times i_z$. Otherwise, if β_1 is the angle to the right side of F_a, the direction of F_s is given by the vector product of $F_a \times -i_z$. The resultant force (F_T) acting on the drone is given by the vector summation of the three forces F_a, F_r, and F_s.

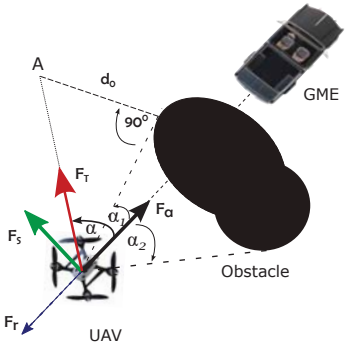

Fig. 1 Top view of the force distribution when the drone is following the GME and encountering a head-on obstacle

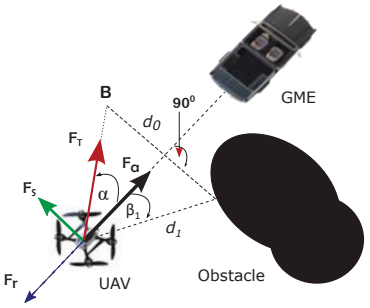

Fig. 2 Top view of the force distribution when the drone is following the GME and encountering a sideway obstacle

A. Force Functions of the Proposed Obstacle Avoidance Technique

The attractive and repulsive exponential force functions proposed in [20] have the advantage of being highly sensitive for a small change of relative displacement and having finite values for all ranges of relative displacements. Therefore, the attractive force F_a and repulsive force F_r presented in [20] are adopted with the following modifications,

$$F_a = \frac{q_1}{|q_1|}\, k_1\, (2 - e^{-c_1\,|q_1|} - e^{-c_2\,|V_1|}) + \frac{q_2}{|q_2|}\, k_2\, (2 - e^{-c_3\,|q_2|} - e^{-c_4\,|V_2|}) + \frac{q_3}{|q_3|}\, k_3\, (2 - e^{-c_5\,|q_3|} - e^{-c_6\,|V_3|});\ k_1 = 0\ if\ F_{s1} = 0, k_2 = 0\ if F_{s2} = 0,\ k_3 = 0\ if\ F_{s3} = 0 \quad (1)$$

$$F_r = \frac{q_o}{|q_o|}\, k_4\, e^{-c_7\,|q_o|}\, (1 + k_5\, e^{-c_8\,|V_o|});\ k_4 = 0\ if\ q_o > d_0,\ k_5 \neq 0\ if\ V_o > 0 \quad (2)$$

where q_1, q_2, q_3 and V_1, V_2, V_3 are the relative displacements and relative velocities between the GME and the drone in the parallel direction of the drone's horizontal plane, perpendicular to the direction of the drone in the horizontal plane, and perpendicular to the direction of the drone in the vertical plane, respectively. The constants k_1, k_2, and k_3 are used to control the maximum attractive force for the corresponding direction where the summation of $k_1 + k_2 + k_3$ gives the maximum resultant attractive force. The positive constants c_1, c_3, c_5 are used to control the maximum relative displacement required to achieve the maximum force. Similarly, the constants c_2, c_4, c_6, and c_8 are included to determine the maximum velocity requirement for the maximum force. The relative displacement and velocity between the obstacles and the drone are represented by q_o and V_o respectively. d_0 is the minimum accepted distance that the drone can approach and be near to the obstacles. The repulsive force factor k_4 is a large positive constant and is the maximum magnitude of the repulsive force that the drone can achieve.

The proposed escape force is activated only when the drone encounters the obstacle and a collision will occur, i.e. when the obstacle is in the range of the drone's collision region. Unlike the existing force field techniques, the proposed obstacle avoidance escape force generates an attractive force for a virtual obstacle goal (point A and B as in Figs. 1 and 2) to change the drone path to prevent any collision. Therefore, the drone does not make any oscillations while avoiding the obstacles due to the low sensitivity of the resultant force in the perpendicular direction to the MGE for a small change of the displacement when the drone is near to the collision region. F_s is defined as,

$$F_s = \begin{cases} k_6\, (1 - e^{-c_9\,|\sqrt{a^2+d_0^2}\, sin(\alpha_1 + tan^{-1}(d_0/a))|}); \\ \qquad 0 < \alpha_1 < \alpha_2\ \&\ d_1 \leq (a_m V_o)/V_m \\ k_7\, (1 - e^{-c_{10}\,|d_0 - (d_1 \sin(\beta_1))|});\ d_1 \sin(\beta_1) \leq d_0 \\ (1 - e^{-c_{12}\,|d_1|})(k_8(1 - e^{-c_{11}\,|V_o|}) + 1); \\ \qquad d_1 \cos(\beta_1) \leq d_0 \end{cases} \quad (3)$$

where k_6, k_7, k_8, and k_9 are the escape force coefficients which determine the maximum value of the escape force. a, and d_1 are the distance to the obstacle from the drone along the drone's heading, and displacement between the drone and the obstacle's surface, respectively. The average velocity that can be reached by the drone in sideway direction is defined as V_m. The positive constants c_9, c_{10}, c_{12} are used to control the maximum relative displacement required to achieve the maximum F_s. Similarly, the constants c_{11} are included to determine the maximum velocity requirement for the maximum F_s. The angles in horizontal plane can be replace from the corresponding angles in vertical plane to calculate the F_s when the minimum distance from the drone to far edge of the obstacle is in the vertical plane.

Fig. 3 shows the force distribution of the proposed obstacle avoidance technique when the drone encounters a head-on obstacle. F_s is automatically activated to maintain a relative displacement of d_0 until the drone passes the obstacle safely. The magnitude of F_s decreases with the sideway distance until it reaches zero when the drone is at d_0 relative displacement from the obstacle's surface. It is then deactivated once the drone reaches a collision free distance ($> d_0$). This enables the obstacle avoidance technique to generate a smooth path without oscillations.

III. Simulation Setup

To validate the proposed obstacle avoidance technique, Gazebo [21] supported PX4 simulation in the loop (PX4-SITL)

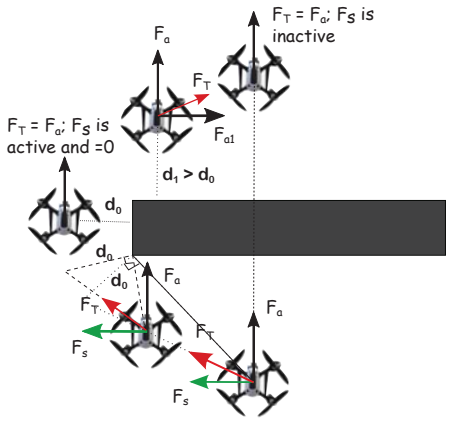

Fig. 3 Force distribution around the obstacle

[22] was used to develop realistic simulation experiments and environments and the Robot Operating System (ROS) [23] was adopted to simulate the GME and drone. The PX4-SITL unmanned aerial vehicle 'Iris' that is equipped with a PX4 autopilot, inertial measurement unit (IMU), GPS receiver, and rp-Lidar is used for the drone simulation. The PX4-SITL unmanned ground vehicle 'rover' is used to simulate the GME with some modifications to enable it to achieve high speeds of up to 20 m/s and provide it with a differential drive control. Besides, bridge-shaped objects, and cylinder-shaped objects are used for examine the performance of the proposed collision avoidance technique when the drone is encountering large sized obstacles. Details of the simulation setup are present in the following subsections.

A. GME and Drone Models

The PX4-SITL 'rover' shown in Fig. 4 (a) is an Ackerman vehicle that has a GPS receiver, but has a limited maximum velocity of 4 m/s and is not capable of driving in a smooth straight-line when using waypoints. Therefore, the vehicle is modified to achieve a maximum velocity of 20 m/s (around 72 km/h) and enable smooth straight-line motion for waypoints navigation. Besides, the PX-4 rover is further modified to enable it to make sharp turns for better maneuvers. The GPS receiver available in the vehicle is used to determine its positional information, where this information is transmitted to the drone via the micro air vehicle link (MAVLink) [24].

The PX4-SITL 'Iris' shown in Fig. 4 (b) is a quadcopter that has a flight controller with PX4 autopilot for autonomous navigation, GPS receiver for positioning data, IMU for accessing heading and speed information, and a MAVLink for receiving the position information of the GME. The GME speed and heading are calculated every 0.3 s. The 'Iris' is not equipped with a distance sensor; therefore, the rp-Lidar available in PX4-SITL is attached to the drone for obstacle detection and distance measurements. The proposed obstacle avoidance path planning technique generated navigational waypoints are provided to the PX4-autopilot for controlling the dynamics of the drone.

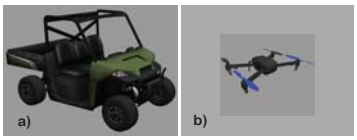

Fig. 4 PX4-SITL (a) 'rover' adopted for simulating the GME, (b) 'Iris' adopted for simulating the drone

B. Obstacle Types

The Gazebo simulation is adopted for simulating static and dynamic obstacles. These obstacles are mainly rectangular and cylindrical surface objects acting as obstacles for the drone but not for the GME as shown in Fig. 5. Besides, another 'Iris' quadcopter has been used as a dynamic obstacle flying towards the drone where its motion is controlled via velocity waypoints.

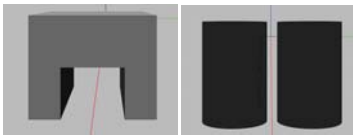

Fig. 5 Obstacles used in the simulation experiments

IV. Simulation Results

To examine the performance of the proposed obstacle avoidance technique, three simulation experiments were developed: two with static obstacles and one with dynamic obstacles. In the first experiment, the GME moves at 10 m/s constant velocity along the X-axis whereas in the second experiment, the GME moves with different velocities in the range from 5 m/s to 20 m/s. In each experiment, the drone and GME start their motions from (0, 0, 0) and (5, 0, 0), respectively. The drone initiates its vertical motion simultaneously as the GME initiates its horizontal motion. The drone initiates its horizontal motion once it reaches point (0, 0, 10) as 10 m is the predefined minimum desired altitude the drone should maintain from the ground level. The accepted displacement that the drone is allowed to approach obstacles is predefined as 1 m. The average velocity of the drone in sideway directions is predefined and set at 5 m/s.

A. Proposed Obstacle Avoidance Performance Evaluation

In the first experiment, a vertical cylinder with a radius of 10 m and height of 15 m was placed at (60, 11.5, 0) to examine the performance of the presented collision avoidance technique when the drone is encountering a sideway object that is not in its collision range. A bridge-shaped object with a length of 25 m, width of 14 m and height of 15 m was placed at (137.5, 3, 0) to evaluate the drone path when a flat surface is encountered and can cause a head-on collision. Besides, another horizontal cylinder with radius of 5 m and length of 24 m was placed at (250, 0, 10) to examine the performances when a curved surface is in the drone's path. Other two cylindrical obstacles each with a radius of 10 m and height of 20 m were placed at (350, -11.5, 0) and (350, 11.5, 0) to observe the drone's path in the presence of symmetrical obstacles. Fig. 6 shows the simulated 3D paths of the GME and drone when encountering static obstacles as the GME moves with 10 m/s speed. The drone does not change its path when passing the first cylindrical object as the displacement between the drone and the cylinder's surface is greater than 1 m. The drone automatically selects to change its horizontal direction in the Y-axis to avoid the bridge-shaped flat surface. This is because the presented collision avoidance generates the escape force in the Y direction as it is the minimum distance path to avoid the obstacle. Similarly, the drone chooses changing of its vertical direction when encountering the curved surface bridge. Finally, the drone successfully follows the GME without changing its path in the presence of symmetrical obstacles. This is because, the displacement between the drone's path and the symmetrical obstacles surfaces are greater than 1 m; therefore, the escape force is zero and the drone does not change its path. The simulation results confirm that the presented obstacle

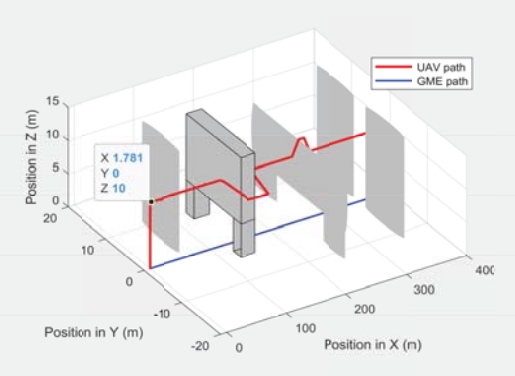

Fig. 6 The drone planned 3D path for different shaped obstacles

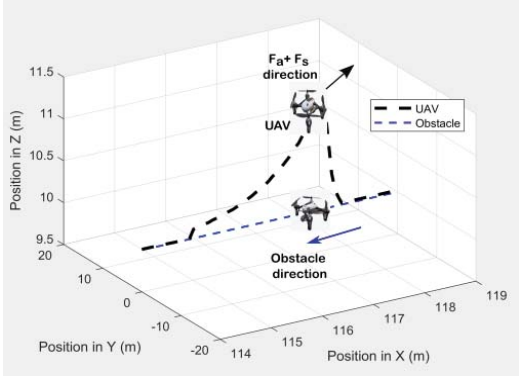

Fig. 8 The drone planned 3D path for avoiding dynamic obstacles while following the GME

avoidance generates a smooth path without oscillations due to the attraction towards the imaginary obstacle point created by F_s.

The second experiment tests the proposed obstacle avoidance technique performance when the GME is moving along the X-direction with different velocities ranging from 5 m/s to 20 m/s and the drone encounters the bridge-shaped flat surface obstacle at (137.5, 3, 0). The obstacle has a length of 25 m, width of 15 m and height of 15 m. Fig. 7 shows the 3D path of the drone when it encounters a head-on collision when following the GME moving at different velocities. As the activating distance of F_s is a function of the relative velocity between the drone and the obstacle; the drone automatically selects the escape force activation point based on the velocity and the turning distance from the obstacle increases for higher drone speeds. Therefore, unlike the existing obstacle avoidance techniques, the presented collision avoidance technique can successfully avoid the obstacle while following GME at high speeds.

In the third experiment, another drone flies towards the path of the drone at 3 m/s speed and 10 m altitude. The GME moves along the X-direction at 5 m/s speed. Fig. 8 shows the drone's planned 3D path for avoiding this dynamic obstacle while following the GME. The drone changes its horizontal direction to avoid the obstacle where the path initial turning position is calculated automatically by using the relative velocity of the drone and the obstacle.

B. Proposed Obstacle Avoidance Performance Comparison to the D-APF and General APF

To compare the performances of the presented collision avoidance technique against the D-APF and the general APF, two cylindrical obstacles each with 15 m height and 5 m radius were placed at (50, -7, 0) and (50, 7, 0) to show the ability of handling symmetrical obstacles. Besides, a bridge-shaped flat surface obstacle with a length of 25 m, width of 14 m and height of 15 m was placed at (137.5, 3, 0) to show the ability of avoiding a head-on obstacle as the minimum distance path is chosen based on the shape of the obstacle. The GME moves along the X-direction at a speed of 5 m/s. The proposed obstacle avoidance technique chooses the shortest path by changing the horizontal displacement to 4 m and follows the movement of the GME at 5 m/s in the positive X-direction as shown in Fig. 9. The D-APF changes its vertical direction and achieves 6 m of displacement from the original path to avoid the bridge-shaped obstacle. Although, the proposed obstacle avoidance technique and the D-APF can avoid symmetrical obstacles, the general APF fails to avoid symmetrical obstacles and to continue following the GME. The proposed obstacle avoidance technique has smooth path compare to the D-APF as shown in in the enlarged section of Fig. 9 shown at the top right of Fig. 9. Similar to the general APFs, the D-APF produces some oscillations when the obstacles are encountered

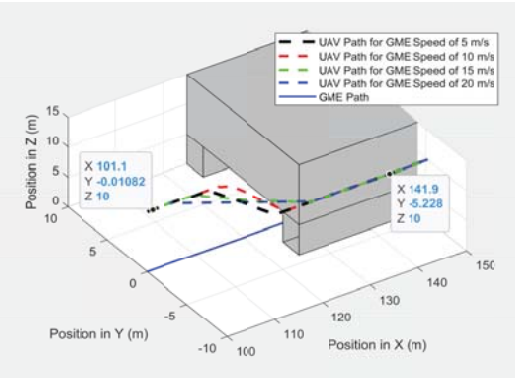

Fig. 7 The drone planned 3D path for a head-on obstacle for different GME speeds

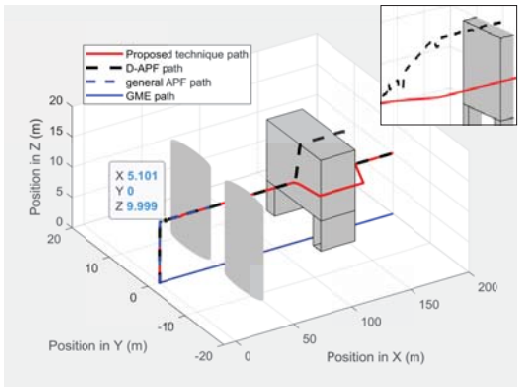

Fig. 9 The drone planned path compared to the D-APF and general APF techniques

due to the simultaneous higher attractive and repulsive forces that are caused by the GME and the obstacle, respectively. For a small change of displacement, the APF generates a higher attractive and repulsive forces which are not equal to each other. Therefore, it produces a couple of oscillations to stabilize or otherwise the oscillations continue until the drone passes the obstacle. The number of oscillations and the peak amplitude of the oscillations increase with the drone speed; therefore; the D-APF can fail to avoid obstacles while pursuing the GME at high speeds. The proposed obstacle avoidance technique avoid this problem by controlling the escape and attractive forces on the drone when obstacles are encountered.

V. Conclusion

This paper presented a three-dimensional obstacle avoidance technique for drones to efficiently avoid dynamic and static obstacles in complex dynamic environments while pursuing ground mobile entities (GMEs). The on-time obstacle avoidance technique generates its obstacle-free and efficient path based on the shape of the obstacles. The proposed escape force can automatically determine the minimum safe distance that the drone can use to approach the obstacles to prevent any collision. It also initiates corrective deviation from the drone's original path based on the relative velocity between the drone and the GME. Besides, the proposed escape force prevents falling in local minima and failure in handling and avoiding symmetrical obstacles. Unlike existing obstacle avoiding techniques, the simulation results confirm that the presented collision avoidance method can find the most efficient and smoothest path for obstacle avoidance while following the GME.

The proposed collision avoidance method has been evaluated in different simulation scenarios. The simulation results confirm that the presented obstacle avoidance technique can successfully avoid static and dynamic obstacles while following the GME moving at high speeds. Besides, the proposed path planning technique is capable of handling high speed dynamic obstacles as the position at which the drone initiates its change of path is determined by the relative velocity between the drone and the obstacles. The performance comparison between the presented collision avoidance technique and the D-APF and general APF shows that the proposed obstacle avoidance technique has outperformed both in terms of obstacle avoidance, smoothness and efficiency of the planned path. Therefore, the presented obstacle avoidance technique is better suited than existing techniques for adoption for the real-world applications.

References

[1] J. T. Butler, "UAVS and ISR Sensor Technology," AIR COMMAND AND STAFF COLL MAXWELL AFB AL, AU/ACSC/033/2001-04, Apr. 2001. Accessed: Apr. 10, 2019. [Online]. Available: https://apps.dtic.mil/docs/citations/ADA407741.

[2] F. Bangkui, Li Yun, R. Zhang, and Fu Qiqi, "Review on the technological development and application of UAV systems," Chinese Journal of Electronics, vol. 29, no. 2, pp. 199-207, Mar. 2020.

[3] J. Y. C. Chen, "UAV-guided navigation for ground robot tele-operation in a military reconnaissance environment," Ergonomics, vol. 53, no. 8, pp. 940–950, Aug. 2010.

[4] S. Sudhakar, V. Vijayakumar, C. Sathiya Kumar, V. Priya, L. Ravi, and V. Subramaniyaswamy, "Unmanned Aerial Vehicle (UAV) based Forest Fire Detection and monitoring for reducing false alarms in forest-fires," Comput. Commun., vol. 149, pp. 1–16, Jan. 2020.

[5] P. Nevavuori, N. Narra, P. Linna, and T. Lipping, "Crop Yield Prediction Using Multitemporal UAV Data and Spatio-Temporal Deep Learning Models," Remote Sens., vol. 12, no. 23, p. 4000, Dec. 2020.

[6] R. H. Kabir and K. Lee, "Wildlife Monitoring Using a Multi-UAV System with Optimal Transport Theory," Appl. Sci., vol. 11, no. 9, p. 4070, Apr. 2021.

[7] S. Chowdhury, A. Emelogu, M. Marufuzzaman, S. G. Nurre, and L. Bian, "Drones for disaster response and relief operations: A continuous approximation model," Int. J. Prod. Econ., vol. 188, pp. 167–184, Jun. 2017.

[8] H. M. P. C. Jayaweera and S. Hanoun, "UAV Path Planning for Reconnaissance and Look-Ahead Coverage Support for Mobile Ground Vehicles," Sensors, vol. 21, no. 13, p. 4595, Jul. 2021.

[9] S. X. Yang and C. Luo, "A Neural Network Approach to Complete Coverage Path Planning," IEEE Trans. Syst. Man Cybern. Part B Cybern., vol. 34, no. 1, pp. 718–724, Feb. 2004.

[10] E. Shan, B. Dai, J. Song, and Z. Sun, "A Dynamic RRT Path Planning Algorithm Based on B-Spline," in 2009 Second International Symposium on Computational Intelligence and Design, Changsha, Hunan, China, pp. 25–29, 2009.

[11] K. H. Sedighi, K. Ashenayi, T. W. Manikas, R. L. Wainwright, and Heng-Ming Tai, "Autonomous local path planning for a mobile robot using a genetic algorithm," in Proceedings of the 2004 Congress on Evolutionary Computation (IEEE Cat. No.04TH8753), Portland, OR, USA, pp. 1338–1345, 2004.

[12] C. C. Wong, H. Y. Wang, and S. A. Li, "PSO-based Motion Fuzzy Controller Design for Mobile Robots," Int. J. Fuzzy Syst., vol. 10, no. 1, p. 9, 2008.

[13] X. Chen and J. Zhang, "The Three-Dimension Path Planning of UAV Based on Improved Artificial Potential Field in Dynamic Environment," in 2013 5th International Conference on Intelligent Human-Machine Systems and Cybernetics, vol. 2, pp. 144–147, Aug. 2013.

[14] S. Back, G. Cho, J. Oh, X.-T. Tran, and H. Oh, "Autonomous UAV Trail Navigation with Obstacle Avoidance Using Deep Neural Networks," J. Intell. Robot. Syst., vol. 100, no. 3–4, pp. 1195–1211, Dec. 2020.

[15] L. Yang, Z. Wei-guo, S. Jing-ping, and L. Guang-wen, "A path planning method based on improved RRT," in Proceedings of 2014 IEEE Chinese Guidance, Navigation and Control Conference, Yantai, China, pp. 564–567, Aug. 2014.

[16] X. Wang and X. Meng, "UAV Online Path Planning Based on Improved Genetic Algorithm," in 2019 Chinese Control Conference (CCC), Guangzhou, China, pp. 4101–4106, Jul. 2019.

[17] D. González, J. Pérez, V. Milanés, and F. Nashashibi, "A Review of Motion Planning Techniques for Automated Vehicles," IEEE Trans. Intell. Transp. Syst., vol. 17, no. 4, pp. 1135–1145, Apr. 2016.

[18] Y. K. Hwang, and N. Ahuja, "A potential field approach to path planning," IEEE Transactions on Robotics and Automation, vol. 8, no. 1, pp. 23-32, Feb. 1992.

[19] Woods, C. Alexander, and M. La. Hung, "Dynamic target tracking and obstacle avoidance using a drone." In International Symposium on Visual Computing, pp. 857-866. Springer, Cham, 2015.

[20] H.M. Jayaweera, and S. Hanoun, "A Dynamic Artificial Potential Field (D-APF) UAV Path Planning Technique for Following Ground Moving Targets." IEEE Access, 8, pp.192760-192776, 2020.

[21] "Gazebo." http://gazebosim.org/ (accessed Apr. 15, 2019).

[22] "Gazebo Simulation PX4 v1.9.0 Developer Guide." https://dev.px4.io/v1.9.0_noredirect/en/simulation/gazebo.html (accessed May 03, 2021).

[23] A. Koubaa, Robot operating system (ROS). New York, NY: Springer Berlin Heidelberg, vol. 1, 2018.

[24] "MAVLink Developer Guide." https://mavlink.io/en/ (accessed Apr. 5, 2019).